Wiley
International Journal of Antennas and Propagation
Volume 2025, Article ID 3445660, 11 pages
https://doi.org/10.1155/ijap/3445660

Research Article

Wideband U-Shaped Wearable Antenna With Defected Ground Structure for Biomedical Wearables

Sanaa Salama[1] **Ashraf Abuelhaija**[2] **Mohammed Hamdan**[2] **Samer Issa**[2] **and Osama Nashwan**[2]

[1]*Department of Biomedical Engineering, Arab American University, Jenin, State of Palestine*
[2]*Department of Electrical Engineering, Applied Science Private University, Amman, Jordan*

Correspondence should be addressed to Sanaa Salama; sanaa.salama@aaup.edu

Received 17 May 2025; Revised 17 June 2025; Accepted 15 July 2025

Academic Editor: Chien-Jen Wang

This study presents a compact, flexible U-shaped wearable antenna with a defected ground structure (DGS) for biomedical applications. Fabricated on a 1 mm polydimethylsiloxane (PDMS) substrate using conductive adhesive tape, the antenna achieves a wide bandwidth of 1.52–5.38 GHz, covering key ISM bands. The DGS enhances impedance matching and stability, while curvature adaptation to a 46 mm arm diameter ensures practical wearability. Simulations in CST and COMSOL demonstrate robust performance near a multilayer human arm phantom, with specific absorption rate (SAR) values compliant with safety standards (< 2 W/kg). Experimental validation confirms the design's reliability, making it a promising solution for wireless body area networks (WBANs) and next-generation biomedical wearables.

Keywords: defected ground structure (DGS); polydimethylsiloxane (PDMS); wearable antenna; wideband antenna; wireless body area networks (WBANs)

1. Introduction

Defected ground structure (DGS) has been widely used due to its simple structural design to enhance various characteristics of microstrip antennas. These enhancements include improved bandwidth, gain, suppression of higher-order harmonics, reduced mutual coupling between adjacent elements, and decreased cross-polarization, thereby improving radiation performance. DGS is typically integrated into the ground plane of planar transmission lines such as microstrip lines, coplanar waveguides (CPWs), and conductor-backed CPWs [1, 2].

DGS is realized by etching specific shapes into the ground plane. Depending on the shape and dimensions of the defect, the shielded current distribution is disturbed, which results in controlled excitation and propagation of electromagnetic (EM) waves through the substrate. When a defect is etched into the ground plane beneath a microstrip line, it alters the line's effective capacitance and inductance by introducing slot resistance, capacitance, and inductance. The defect's shape can vary from simple to complex geometries to achieve better performance.

DGS has been employed in various applications, including microwave filters [3–5], power amplifiers [6], power dividers [7], transmission lines [8], and microstrip antennas [9, 10]. A novel DGS design used as an electromagnetic band gap (EBG) structure for printed antenna and circuit applications was introduced in [11]. This design features concentric annular rings with equal widths and spacings. It was designed for operation at 10 GHz and fabricated on a Taconic PTFE substrate (dielectric constant of 2.33 and thickness of 1.575 mm).

A split-ring resonator–based DGS with an integrated lumped-element capacitor was presented in [12] for a wide bandpass microstrip filter operating from 1 to 2.4 GHz. Another DGS design, consisting of two rectangular areas connected by a slot, was introduced in [13, 14]. The effect of a dumbbell-shaped DGS on reducing the size of a microstrip patch antenna was also investigated in [13].

A modified ultra-wideband (UWB) patch antenna with a defected ground plane was proposed in [15]. The antenna, with dimensions of $22 \times 30 \times 1.62\,\mathrm{mm}^3$, is printed on an FR-4 substrate and operates over a wide bandwidth from 4 to 13 GHz. The structure is fed by a CPW feed line designed on a Taconic substrate. A defected ground plane structure was also introduced in [16] for UWB applications. This antenna, with dimensions of $20 \times 25 \times 1.5\,\mathrm{mm}^3$, is likewise printed on an FR-4 substrate. The inclusion of the defected ground plane led to enhanced antenna characteristics, achieving a gain of 5.1 dB and an efficiency of 89%. The implementation of the DGS resulted in an impedance bandwidth of 95%, covering the frequency range from 3.4 to 9.66 GHz. In [17], a miniaturized metamaterial-based microstrip antenna, printed on silver nanoparticle ink on a $20 \times 10\,\mathrm{mm}^2$ polymer substrate, was presented. The proposed design effectively reduces back radiation toward the human body, making it a good candidate for biomedical wireless devices. In [18], two types of dual-band wearable planar dipole antennas were proposed: one printed on a conventional ground plane and the other on an EBG structure. The wearable antenna with the EBG structure reduced specific absorption rate (SAR) on the human body and improved the antenna gain by 4.45 dBi. The SAR in [19] was reduced by designing a 2.4 GHz wearable planar patch antenna with EBG ground plane. The antenna, measuring $113 \times 96.4 \times 3\,\mathrm{mm}^3$, was constructed using Zelt as the conductive material and wash cotton as the substrate. The 2.45 GHz coplanar wearable antenna presented in [20] utilized a $30 \times 30\,\mathrm{mm}^2$ EBG structure to reduce the SAR. At the 2.45 GHz frequency band, the SAR value achieved was 0.0344 W/kg. Metamaterial-based wearable antennas proposed in [21–24] were aimed to reduce SAR values and enhance antenna gain. In [25], a compact two-element textile MIMO antenna was designed with improved isolation of more than 21.1 dB, achieved by introducing open-ended slots and shorting pins into the ground plane. An eight-port MIMO antenna with a defected ground plane for improved impedance matching was proposed in [26].

This paper proposes a wideband U-shaped wearable antenna for medical applications, featuring unique properties that distinguish it from previously reported designs. The antenna has a low-profile structure and is fabricated on a flexible substrate, allowing it to conform easily to the curvature of various parts of the human body. Its simple design facilitates easy and cost-effective fabrication. The antenna operates over a wide bandwidth within the Industrial, Scientific, and Medical (ISM) frequency band, providing flexibility in selecting an appropriate operating frequency. The radiating element is integrated with a DGS to ensure stable performance when worn on the human body and to meet safety compliance requirements.

This paper is organized as follows. The Introduction discusses the advantages of employing DGSs in antenna design and highlights their practical applications. Section 2 describes the methodology for designing a wideband U-shaped wearable antenna incorporating DGS, including the design evolution stages and corresponding S-parameter results. Section 3 analyzes the effect of varying the distance between the antenna and a human arm model on the antenna's performance. It also presents the 1 and 10 g SAR distributions on the arm model at 2.45 GHz and 5 GHz. Section 4 validates the proposed antenna design by comparing simulation results obtained from CST and COMSOL.

2. Methodology

The wideband U-shaped wearable antenna developed in this study is an evolution of a previously reported U-shaped patch fabric antenna [27], enhanced through the integration of a DGS. This configuration is depicted in Figures 1(a) and 1(b). The antenna's performance was assessed using CST Microwave Studio, revealing wideband operation spanning from 1.52 to 5.38 GHz. Designed on a polydimethylsiloxane (PDMS) substrate, the antenna benefits from the material's flexibility and favorable dielectric properties, including a thickness of 1 mm, a relative permittivity of 2.75, and negligible conductivity. The antenna's compact dimensions measure $50 \times 28\,\mathrm{mm}^2$, as illustrated in Figure 1. A copper tape with a conductivity of 5.8×10^7 S/m serves as the radiating material. To enhance impedance matching and broaden the operational bandwidth, a rectangular slot was introduced at the center of the ground plane. This modification results in a U-shaped ground plane, forming the DGS configuration shown in Figure 1(b). The DGS effectively alters the current distribution, improving the antenna's return loss across the targeted frequency range. This design approach aligns with contemporary trends in wearable antenna development, where flexible substrates like PDMS and conductive adhesive tape are employed to achieve compact, efficient, and broadband performance suitable for integration into wearable devices.

2.1. Simulation Environment.

Wearable antennas necessitate specialized simulation conditions due to their interaction with complex biological tissues, distinguishing them from antennas operating in free space. In this study, simulations were conducted by positioning the antenna on a multilayer phantom model designed to replicate the human arm, as depicted in Figure 2(a). This model comprises four layers—bone, muscle, fat, and skin—illustrated in Figure 2(b). Table 1 provides detailed information on the conductivity, density, permittivity, and thickness of each layer.

To accurately simulate the real-life positioning of the antenna on the arm, the bending process was carried out in CST Microwave Studio by curving the proposed design to match the arm model's diameter ($d = 46$ mm). This approach ensures that the antenna conforms to the curvature of the arm, allowing for a realistic assessment of its performance in wearable applications.

Such detailed modeling is crucial for evaluating key performance metrics, including impedance matching, radiation patterns, and SAR, which are directly influenced by the antenna's proximity to human tissues. Accurate

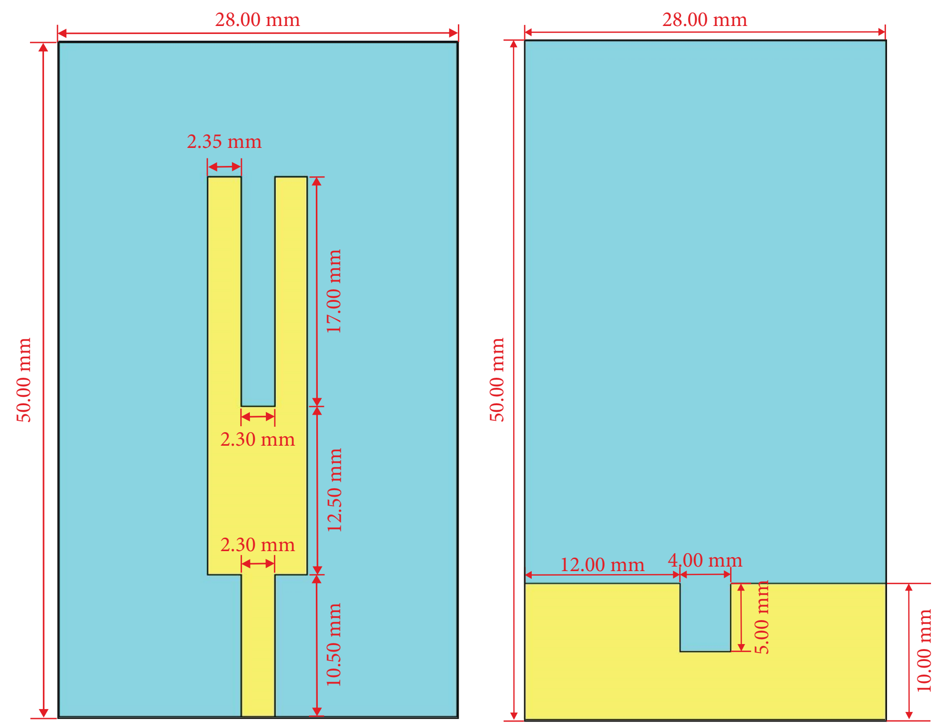

(a) (b)

Figure 1: The geometry for the proposed wideband U-shaped wearable antenna with DGS: (a) front view [27] and (b) back view.

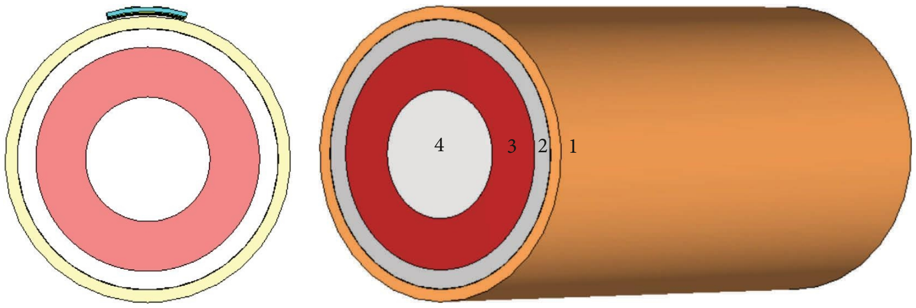

(a) (b)

Figure 2: (a) Simulation setup and (b) the four layers of the arm model.

Table 1: Material properties of the human arm model [21, 28].

Layer	Thickness radius (mm)	Relative permittivity (ε_r)	Conductivity σ (S/m)	Density (kg/m^3)
1. Skin	2	38	1.46	1001
2. Fat	3	5.28	0.1	900
3. Muscle	8	52.72	1.73	1006
4. Bone	10	18.54	0.8	1008

simulations help predict potential detuning effects and efficiency losses, ensuring the antenna's reliability and safety in practical wearable scenarios.

2.2. Design Process. The performance of wearable antennas is significantly influenced by their proximity to the human body, necessitating multiple design iterations to achieve optimal functionality. Key objectives in this optimization process include achieving wideband frequency operation and improving impedance matching. The design evolution of the antenna follows a five-stage process, as illustrated in Figure 3(a). Each stage introduces specific modifications aimed at enhancing performance metrics. The reflection coefficient (S_{11}) results corresponding to each design stage are compared

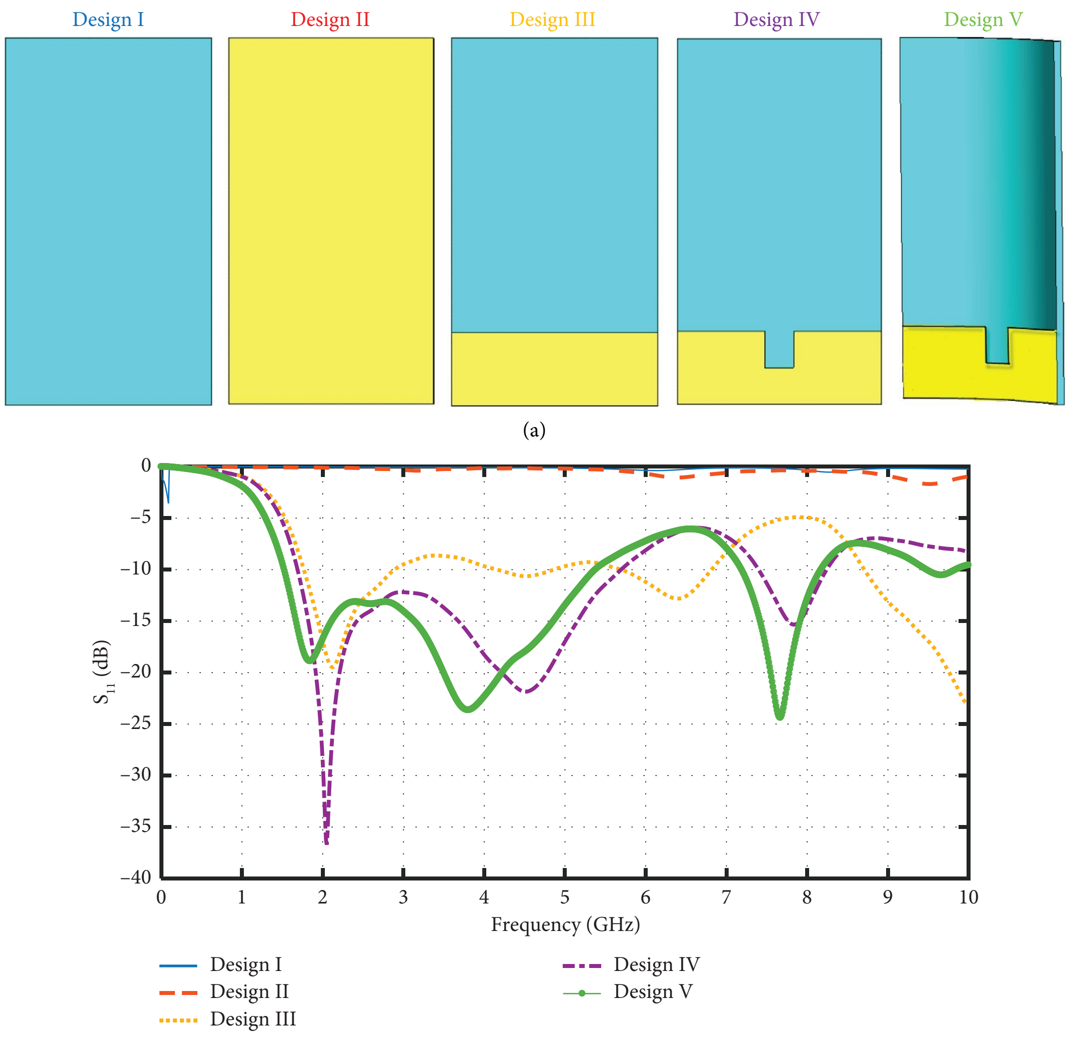

(a)

(b)

FIGURE 3: (a) Evolution of the wideband flexible U-shaped patch antenna and (b) the reflection coefficient for each design.

in Figure 3(b), providing insights into the impedance matching improvements achieved through iterative design refinements.

Such iterative refinements are crucial for wearable antennas, as they must maintain performance despite the detuning effects caused by the lossy and high-permittivity nature of human tissues. By systematically adjusting design parameters, the developed antennas can offer reliable performance in real-world wearable applications.

2.2.1. Design I (Antenna Without Ground). The initial configuration of the antenna features a U-shaped patch situated on the top layer, as depicted in Figure 1(a), without the inclusion of a ground plane on the bottom layer. In this setup, the antenna remains flat, with no bending applied, and is positioned 1 cm above the arm model. This preliminary design resulted in two mismatched operating frequencies at 6.12 and 8.28 GHz, indicating suboptimal impedance matching and limited suitability for the intended wearable application.

2.2.2. Design II (Antenna With Full Ground). In the second design iteration, a full ground plane was introduced on the bottom layer, replacing the absence of a ground plane in Design I. This modification led to a downward shift in the previously mismatched operating frequencies, bringing them to 3.14 and 6.41 GHz. However, a new mismatched operating frequency emerged at 9.51 GHz.

The antenna's impedance characteristics reveal distinct resonant behaviors across its operating frequencies. At the first resonant frequency, the antenna exhibits characteristics of a series resonant circuit. Conversely, at the second and third resonant frequencies, the antenna behaves like a parallel resonant circuit.

2.2.3. Design III (Antenna With Partial Ground). In this design phase, the antenna's bottom layer incorporates a partial ground plane, replacing the full ground plane used in the previous iteration. This alteration introduces a reactive load that significantly influences the antenna's performance. Specifically, the first resonant frequency shifts downward to

2.14 GHz, the second to 4.52 GHz, and the third to 6.39 GHz. Additionally, impedance matching is enhanced at these frequencies, leading to improved return loss characteristics.

2.2.4. Design IV (Antenna With DGS Configuration). In this design phase, a DGS is incorporated into the antenna's bottom layer. The introduction of the DGS adds a matched resonance frequency between 4 and 5 GHz. This modification significantly enhances impedance matching across a broad frequency range, resulting in wideband operation spanning from 1.69 to 5.67 GHz.

DGS unit can be analyzed by a parallel R, L, and C resonant circuit (Figure 4). A resistance R is added to the LC circuit to model the radiation, conductor, and dielectric losses. The capacitance C, inductance L, and resistance R can be calculated as [29]

$$C = \frac{\omega_c}{2Z_o\left(\omega_o^2 - \omega_c^2\right)}, \tag{1}$$

$$L = \frac{1}{4\pi^2 f_o^2 C}, \tag{2}$$

$$R(\omega) = \frac{2Z_o}{\sqrt{1/\left|S_{11}(\omega)\right|^2 - \left(2Z_o(\omega C - 1/\omega L)\right)^2 - 1}}. \tag{3}$$

2.2.5. Design V (Curved Antenna With DGS Configuration). In this design iteration, the antenna is contoured to conform to the curvature of the arm model with a diameter of 46 mm. This bending aligns the antenna's structure with the arm's shape, effectively simulating real-world wearable conditions. As a result of this curvature, the antenna's broadband frequency response shifts toward lower frequencies, now covering a range from 1.52 to 5.38 GHz.

3. Equivalent Circuit

Wideband antennas are defined by the presence of multiple resonant frequencies in close spectral proximity, where the partial overlap of adjacent resonances produces a continuous and broad operational bandwidth. This overlapping behavior is intrinsic to wideband operation, supporting efficient power transfer and stable impedance characteristics across a wide frequency range. To model the EM response of individual resonant modes, parallel RLC circuits are commonly employed, capturing the localized frequency-dependent impedance behavior. In the design and modeling of wideband antennas, these parallel RLC resonators are arranged in a series configuration to collectively approximate the antenna's broadband impedance profile. This serial composition effectively accounts for the interaction between neighboring resonances and facilitates a modular representation of the antenna's frequency response. Each resonator contributes to a distinct segment of the spectrum, and their combined behavior ensures smooth impedance transitions and sustained radiation performance across the full bandwidth.

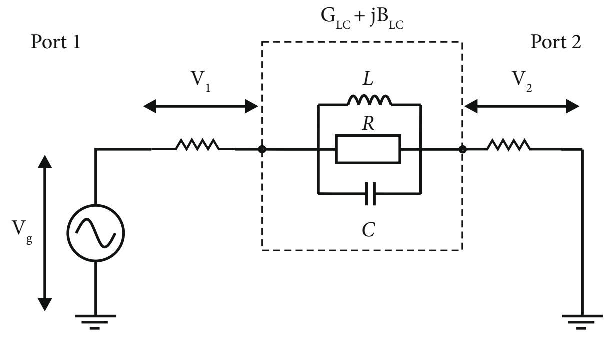

Figure 4: *RLC* equivalent circuit for unit DGS.

To enable a more detailed and accurate characterization of the proposed antenna's performance, an equivalent circuit model is constructed using Advanced Design System (ADS), a widely adopted electronic design automation (EDA) platform specialized in high-frequency circuit simulation. The model architecture is based on the degenerated Foster canonical form, a recognized approach for representing passive networks. This formulation is particularly effective in capturing the broadband impedance behavior typical of UWB antennas [30–32].

The modeling process commences with the careful initialization of circuit component values, including inductance, capacitance, and resistance. These parameters are iteratively optimized through simulation to ensure a close match between the EM response of the antenna and the behavior of the equivalent circuit. Specifically, alignment of the reflection coefficient (S_{11}) profiles obtained from both full-wave EM simulations and circuit-level simulations within ADS is used as the primary criterion for validation. The resulting optimized equivalent circuit model, illustrated in Figure 5, accurately replicates the antenna's performance across the target frequency range. To accurately emulate the behavior of the proposed wideband antenna, four dominant resonant modes are modeled using a series-connected arrangement of parallel LC tank circuits. Each tank circuit comprises an inductor and capacitor in parallel, with an associated resistor representing the radiation resistance corresponding to that specific resonance. This configuration enables a realistic approximation of the antenna's radiation properties and impedance characteristics across the operating bandwidth.

The validity of the equivalent circuit model is confirmed by comparing its results with those obtained from full-wave EM simulations. As shown in Figure 6, the reflection coefficient (S_{11}) curves from both approaches exhibit a high degree of agreement, demonstrating the model's accuracy in capturing the essential performance characteristics of the antenna. Furthermore, the detailed values of all circuit components—inductors, capacitors, and resistors—are provided in Table 2, offering a comprehensive reference for replication and further analytical studies.

4. Simulation Results

4.1. Impacts of Arm Loading. In this design phase, the wideband U-shaped wearable antenna is tailored to operate effectively within the 1.52–5.38 GHz frequency range when

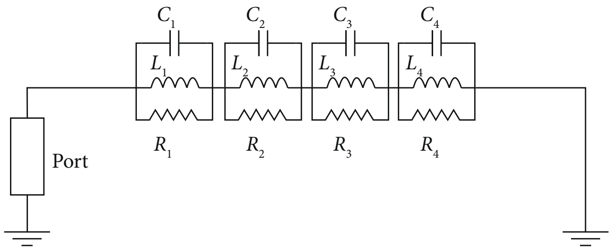

Figure 5: Proposed equivalent circuit model for wideband U-shaped wearable antenna with DGS.

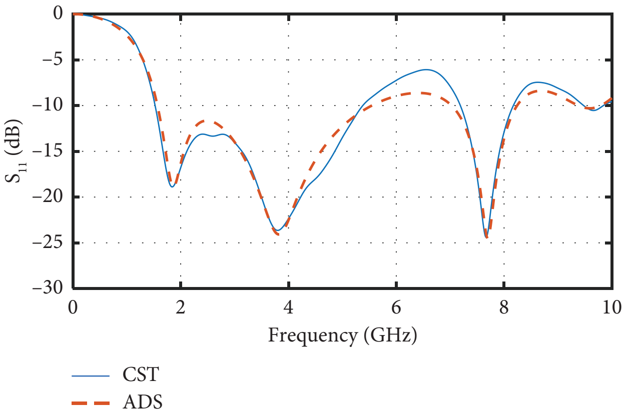

Figure 6: Simulated S_{11} parameter (CST and ADS).

positioned directly on an arm model, as depicted in the simulation setup in Figure 2. The simulations involved placing the antenna in close contact with the arm model, which comprises multilayer tissues exhibiting high dielectric properties, as detailed in Table 1. To assess the impact of proximity on antenna performance, simulations were conducted at varying distances between the antenna and the arm model. The results, illustrated in Figure 7, reveal that as the separation distance increases, the antenna's wideband characteristics diminish. At a 1 mm distance, the antenna maintains its broad frequency coverage. However, at 2 mm, while the wideband behavior persists, the bandwidth narrows. Beyond 3 mm, the wideband characteristic transitions into a dual-band response. This behavior can be attributed to the high permittivity and lossy nature of human tissues, which influence the antenna's impedance matching and resonant frequencies. Proximity to the body enhances capacitive coupling, leading to better impedance matching and broader bandwidth. As the distance increases, this coupling weakens, resulting in reduced bandwidth and altered frequency response. Understanding these effects is crucial for optimizing wearable antenna designs, ensuring reliable performance across intended frequency bands under various physical configurations encountered during actual use.

4.2. SAR Evaluation. The SAR measures the amount of RF energy absorbed by biological tissue when exposed to EM fields, expressed in watts per kilogram (W/kg). SAR can be determined either at a particular tissue location or averaged across a larger area. It plays a critical role in evaluating the safety of tissues under EM exposure. Two major standards govern SAR limits: IEEE C95.1-1999 specifies a maximum of 1.6 W/kg averaged over 1 g of tissue [33], while IEEE C95.1-2005 permits up to 2 W/kg averaged over 10 g [34]. The Federal Communications Commission (FCC) [35] adopts the 1 g averaging standard, whereas the International Commission on Non-Ionizing Radiation Protection (ICNIRP) recommends averaging over 10 g [36]. To meet these regulatory requirements, wearable antennas must function at low power levels.

Figure 8(a) shows the top view of the 1 g-SAR distribution on the human arm model when exposed to an EM field at 2.45 GHz with an accepted power of 15 mW. The highest SAR values (indicated in red) are concentrated at the center, highlighting the region of maximum energy absorption. The peak value reaches approximately 1.33 W/kg, demonstrating that the antenna remains well within safety limits while ensuring efficient energy usage. Figure 8(e) provides the corresponding side view, where the maximum SAR values are observed in the first two layers of the arm model, gradually decreasing with depth.

Figure 8(b) presents the 1 g-SAR distribution (top view) at 5 GHz with an accepted power of 10 mW. The maximum SAR value reaches about 1.55 W/kg, remaining compliant with established safety standards. Figure 8(f) shows the side view for the same conditions, exhibiting a similar absorption profile as observed at 2.45 GHz.

Figure 8(c) illustrates the 10 g-SAR distribution (top view) for the arm model at 2.45 GHz with an accepted power of 50 mW. The peak SAR value reaches approximately 2 W/kg, confirming compliance with EM exposure regulations. Figure 8(g) depicts the corresponding side view, showing that energy absorption begins to diminish starting from the third layer and continues to decrease toward the deeper tissues.

Figure 8(d) displays the 10 g-SAR distribution (top view) at 5 GHz with an accepted power of 40 mW. The maximum SAR value again approaches 2 W/kg, indicating adherence to safety standards. Figure 8(h) presents the side view under the same conditions, revealing a comparable energy absorption pattern to that observed for the 10 g-SAR distribution at 2.45 GHz.

5. Design Validation

5.1. S-Parameter Characteristics. To validate the simulation results obtained from CST, a comparison was performed between the CST and COMSOL simulation outcomes. Figure 9 presents the reflection coefficients obtained from both software platforms. The results demonstrate good agreement, confirming the wideband characteristics of the proposed wearable antenna. Specifically, both simulations indicate a wide bandwidth of 3.86 GHz, ranging from 1.52 to 5.38 GHz. This consistency between the two different simulation tools strengthens the reliability and accuracy of the antenna design. Minor discrepancies observed in the reflection coefficient curves can be attributed to differences in meshing techniques, solver algorithms, and numerical

Table 2: The respective values of the electrical components used in the equivalent circuit (units: Ω, nH, and pF).

Element	R_1	L_1	C_1	R_2	L_2	C_2	R_3	L_3	C_3	R_4	L_4	C_4
Value	45.5	0.1	4.06	41.4	1.52	1.07	37.5	1.69	5.2	27.2	0.1	2.54

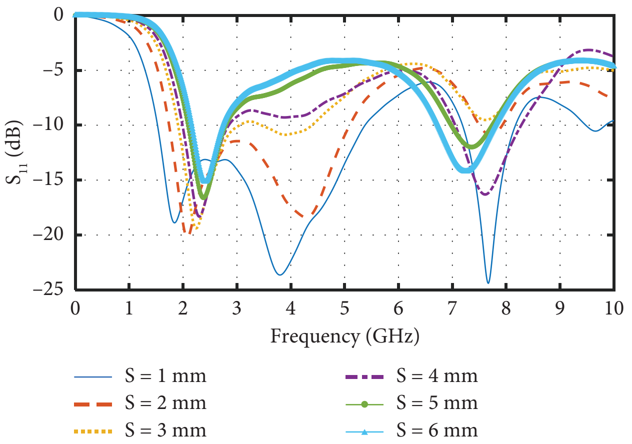

Figure 7: The reflection coefficient as a function of the distance from the phantom.

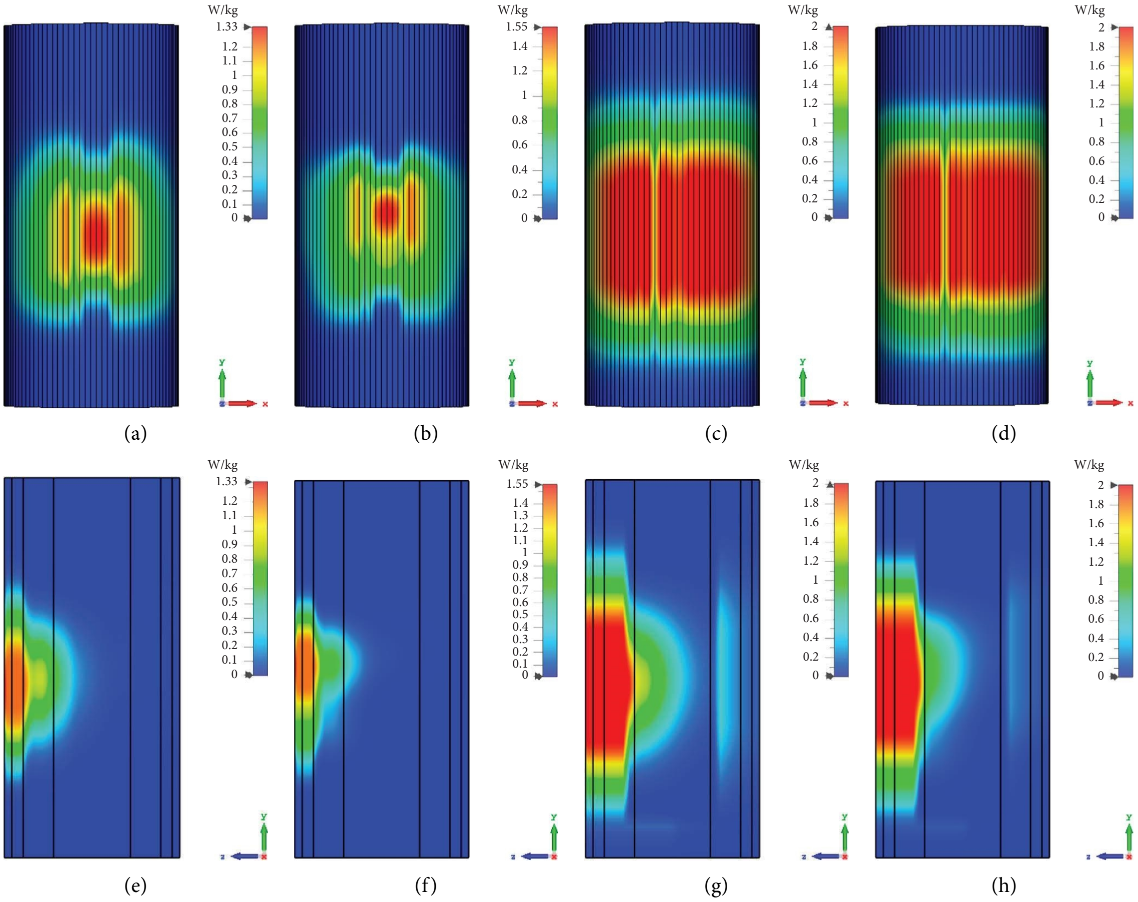

(a) (b) (c) (d)

(e) (f) (g) (h)

Figure 8: SAR distribution of the wideband U-shaped wearable antenna at (a) 1 g-SAR at 2.45 GHz (top view), (b) 1 g-SAR at 5 GHz (top view), (c) 10 g-SAR at 2.45 GHz (top view), (d) 10 g-SAR at 5 GHz (top view), (e) 1 g-SAR at 2.45 GHz (side view), (f) 1 g-SAR at 5 GHz (side view), (g) 10 g-SAR at 2.45 GHz (side view), and (h) 10 g-SAR at 5 GHz (side view).

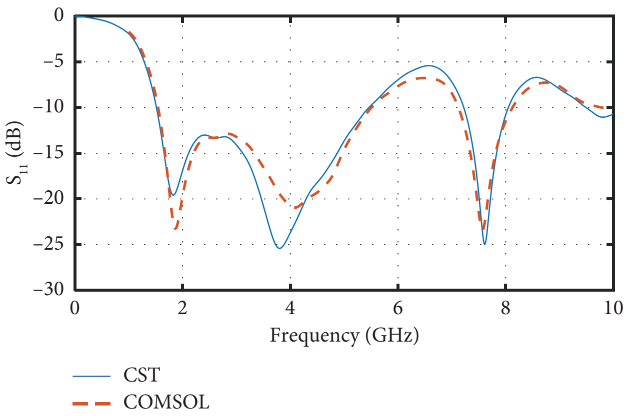

Figure 9: Comparison of S_{11} results between CST and COMSOL.

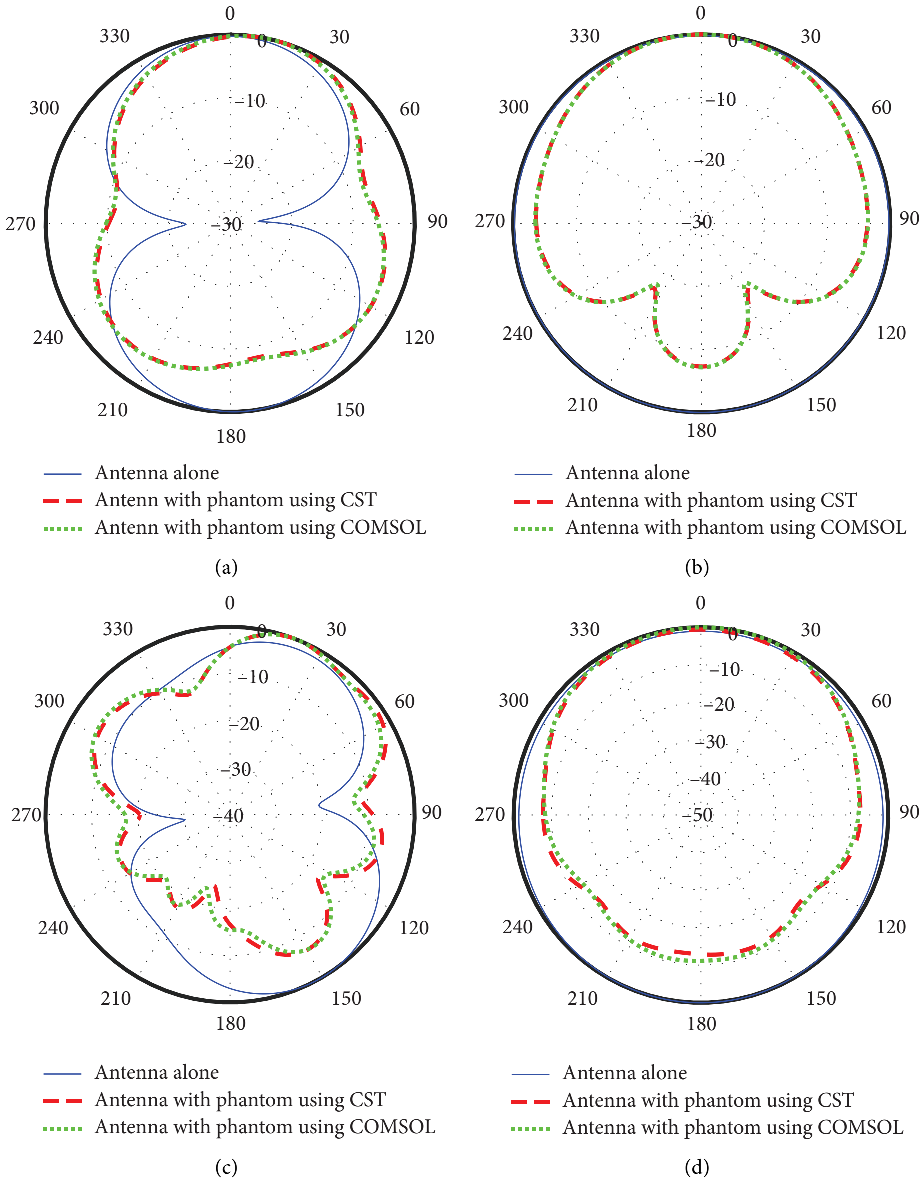

(a)

(b)

(c)

(d)

Figure 10: Simulation of radiation pattern characteristics: (a) E-plane at 2.45 GHz, (b) H-plane at 2.45 GHz, (c) E-plane at 5 GHz, and (d) H-plane at 5 GHz.

approximations inherent to each software. Nevertheless, the strong correlation between the CST and COMSOL results validates the robustness of the proposed design approach and highlights its suitability for wideband wearable applications, ensuring stable performance across the targeted frequency range.

5.2. Radiation Patterns. The performance of wireless devices is heavily impacted by their radiation patterns. Figure 10 presents the radiation patterns of the proposed wideband U-shaped wearable antenna at 2.45 and 5 GHz across three scenarios: the antenna alone, the antenna near a phantom simulated in CST, and the antenna near a phantom simulated in COMSOL.

Figures 10(a) and 8(b) illustrate the E-plane and H-plane patterns at 2.45 GHz. When measured alone (blue solid line), the antenna exhibits an omnidirectional radiation pattern, typical for wearable applications seeking consistent coverage. However, when placed near the phantom, simulating on-body conditions, the pattern becomes more directive due to the influence of human tissue. High radiation efficiency is difficult to maintain because biological tissues absorb EM waves, as modeled by the phantom. The antenna achieves an average radiation efficiency of approximately −10.31 dB (0.093).

Figures 10(c) and 8(d) show the E-plane and H-plane at 5 GHz. Again, the standalone antenna (blue solid line) produces an almost omnidirectional pattern. When placed near the phantom, both CST (red dashed line) and COMSOL (green dotted line) simulations reveal distortions and multiple lobes, resulting in a more directive pattern with minor shifts in elevation angle. These changes are due to dielectric loading and absorption by the phantom. At 5 GHz, radiation efficiency further drops to around −17.27 dB (0.0187).

Antenna parameters such as gain and efficiency are summarized in Table 3. The table shows that both gain and efficiency decrease as the frequency increases. This behavior can be attributed to the increased absorption of EM waves by the dielectric load at higher frequencies. As the frequency rises, the dielectric material tends to exhibit greater losses, which in turn reduces the radiated power and overall antenna performance. These findings highlight the importance of carefully optimizing the antenna design to minimize losses and ensure satisfactory performance across the intended frequency band.

Despite the distortions, the general shape of the radiation pattern remains fairly consistent between CST and COMSOL results, demonstrating that the antenna maintains stable directional performance when worn.

Table 3: Antenna parameters (gain and efficiency) at different operational frequencies.

Frequency (GHz)	Gain (dBi)	Efficiency
1.52	−6.37	0.1138
2.00	−6.31	0.139
2.45	−5.57	0.093
3	−7.29	0.063
3.5	−6.65	0.058
4	−9.54	0.027
4.5	−11.9	0.015
5	−10.5	0.018
5.4	−8.18	0.025

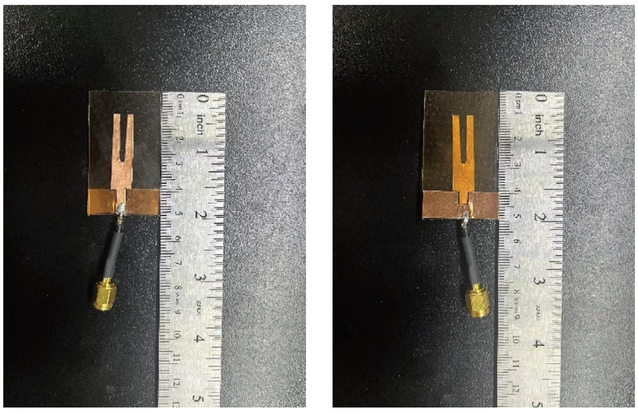
(a) (b)

Figure 11: The prototype for the proposed wideband U-shaped wearable antenna with DGS: (a) front view and (b) back view.

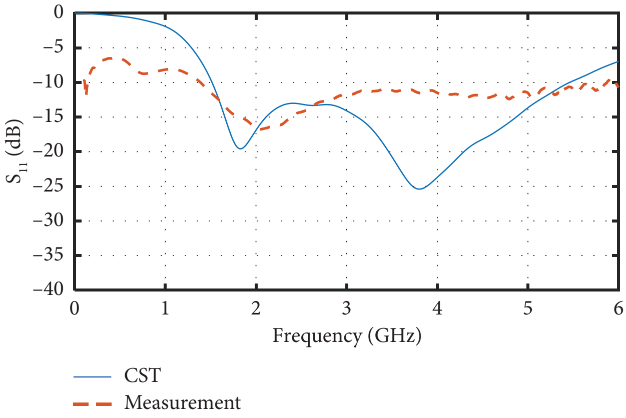

Figure 12: Comparison of S_{11} results between CST and measurement.

6. Fabrication and Measurements of the Proposed Wideband U-Shaped Wearable Antenna With DGS

The prototype of the proposed wideband U-shaped wearable antenna with DGS is shown in Figure 11. It has been fabricated using conductive adhesive tape, which is pasted onto a PDMS substrate ($\varepsilon_r = 2.75$, $\tan\delta = 0.025$) with a thickness of 1 mm. The dimensions of the antenna, as well as the radiating material and ground plane, are the same as those mentioned in Figure 1. A 50 Ω short coaxial cable has been soldered to the antenna to serve as the antenna port. To measure the reflection coefficient, a vector network analyzer (VNA) covering frequencies up to 6 GHz has been used to cover the antenna's operational range. The antenna was positioned on the human arm by curving it to match the arm's curvature. Figure 12 shows the S_{11} results for both the simulated and measured cases. An acceptable agreement is observed between the two, with the covered bandwidths being almost the same. For the simulated case, the wideband operation spans from 1.52 to 5.38 GHz, whereas for the measured case, it spans from 1.4 to 5.6 GHz. The difference in behavior between the simulated and measured results can be attributed to the uncertainty in the curving angle of the antenna on the arm. In addition, the thickness of the arm model layers used in the simulation might differ from that of the actual arm used in the measurement.

7. Conclusion

The proposed wideband U-shaped wearable antenna with a DGS successfully addresses the challenges of designing antennas for biomedical wearable applications. By leveraging a flexible PDMS substrate and conductive textile, the antenna achieves a broad operational bandwidth while maintaining compact dimensions. The integration of DGS significantly enhances impedance matching and bandwidth, ensuring stable performance even when bent to conform to the human arm. Comprehensive simulations validate the antenna's compliance with SAR safety limits, demonstrating its suitability for real-world wearable use. The design's robustness is further confirmed through cross-software validation between CST and COMSOL, with consistent results across key performance metrics. Experimental measurements further supported the simulation results, demonstrating the antenna's practical viability for real-world wearable applications. While DGS can introduce potential instability in radiation patterns and gain, in this work, the DGS geometry and placement were carefully optimized to ensure stable radiation characteristics suitable for wearable biomedical applications.

Data Availability Statement

The data that support the findings of this study are available from the corresponding author upon reasonable request.

Conflicts of Interest

The authors declare no conflicts of interest.

Funding

No funding was received for this manuscript.

References

[1] H. W. Liu, Z. F. Li, and X. W. Sun, "A Novel Fractal Defected Ground Structure and Its Application to the Low-Pass Filter," *Microwave and Optical Technology Letters* 39, no. 6 (2003): 453–456, https://doi.org/10.1002/mop.11246.

[2] D.-J. Woo, T.-K. Lee, J.-W. Lee, C.-S. Pyo, and W.-K. Choi, "Novel U-Slot and V-Slot DGSs for Bandstop Filter With Improved Q Factor," *IEEE Transactions on Microwave Theory and Techniques* 54, no. 6 (2006): 2840–2847, https://doi.org/10.1109/TMTT.2006.875450.

[3] S. O. Coumar, "Miniaturized DGS Based Multi-Band Pass Filters for Satellite Applications," *Journal of Ambient Intelligence and Humanized Computing* 13, no. 1 (2022): 241–249, https://doi.org/10.1007/s12652-021-02898-3.

[4] G. Soundarya and N. Gunavathi, "Compact Dual-Band SIW Band Pass Filter Using CSRR and DGS Structure Resonators," *Progress In Electromagnetics Research Letters* 101 (2021): 79–87, https://doi.org/10.2528/pierl21091301.

[5] Y. Jiang, L. Meng, and G. Yang, "A Novel Dual-Mode Dual-Band Bandpass Filter With DGS Structure," in *2015 Asia-Pacific Microwave Conference (APMC)* (Nanjing, China, December 2015), 1–3, https://doi.org/10.1109/APMC.2015.7412976.

[6] V. Radisic, Y. Qian, and T. Itoh, "Broadband Power Amplifier Using Dielectric Photonic Bandgap Structure," *IEEE Microwave and Guided Wave Letters* 8, no. 1 (1998): 13–14, https://doi.org/10.1109/75.650973.

[7] J. S. Lim, S. W. Lee, C. S. Kim, J. S. Park, D. Ahn, and S. W. Nam, "A 4:1 Unequal Wilkinson Power Divider," *IEEE Microwave and Wireless Components Letters* 11, no. 3 (2001): 124–126.

[8] S. G. Jeong, D. Hwang, Y. C. Jeong, and C. D. Kim, "Amplifier Design Using/spl Lambda//4 High Impedance Bias Line With Defect Ground Structure (DGS)," in *2002 IEEE MTT-S International Microwave Symposium Digest (Cat. No.02CH37278)* (Seattle, WA, 2002), https://doi.org/10.1109/MWSYM.2002.1011854.

[9] E. Sarva Rameswarudu and P. V. Sridevi, "Compact Microstrip Defected Ground Structured Antenna for Reduction of Harmonics and Cross Polarized Radiations," *International Journal of Applied Engineering Research* 10, no. 19 (2015): 40396–40399.

[10] R. Pandhare, P. L. Zade, and M. P. Abegaonkar, "Harmonic Control by Defected Ground Structure on Microstrip Antenna Array," *Indian Journal of Science and Technology* 8, no. 35 (2015): https://doi.org/10.17485/ijst/2015/v8i35/79640.

[11] D. Guha, S. Biswas, M. Biswas, J. Y. Siddiqui, and Y. M. M. Antar, "Concentric Ring-Shaped Defected Ground Structures for Microstrip Applications," *IEEE Antennas and Wireless Propagation Letters* 5, no. 1 (2006): 402–405, https://doi.org/10.1109/lawp.2006.880691.

[12] Z.-Z. Hou, "Novel Wideband Filter With a Transmission Zero Based on Split-Ring Resonator DGS," *Microwave and Optical Technology Letters* 50, no. 6 (2008): 1691–1693, https://doi.org/10.1002/mop.23452.

[13] A. K. Arya, M. V. Kartikeyan, and A. Patnaik, "Efficiency Enhancement of Microstrip Patch Antenna with Defected Ground Structure," in *IEEE Proceedings Recent Advanced in Microwave Theory and Applications (MICROWAVE-08)* (Jaipur, India, November 2008), 729–731, https://doi.org/10.1109/AMTA.2008.4763036.

[14] R. Hamid, D. Oskouei, and J. Khalilpour, "Neural Model for Modeling of Dumbbell Shape Defected Ground Structure," in *PIERS Proceedings* (Suzhou, China, 2011).

[15] R. H. Mahdi, A. Alsudani, M. Q. Abdalrazak, H. A. Abdulnabi, and Abdulnabi, "Design of Defective Ground Plane Modified Microstrip Patch Antenna for Ultra-Wideband Applications," *TELKOMNIKA (Telecommunication Computing Electronics and Control)* 22, no. 1 (2024): 34–41, https://doi.org/10.12928/TELKOMNIKA.v22i1.25577.

[16] S. Baudha and M.V. Yadav, "A Novel Design of a Planar Antenna With Modified Patch and Defective Ground Plane for Ultra-Wideband Applications," *Microwave and Optical Technology Letters* (2019): 1–8, https://doi.org/10.1002/mop.31716.

[17] A. Al-Adhami and E. Ercelebi, "A Flexible Metamaterial Based Printed Antenna for Wearable Biomedical Applications," *Sensors* 21, no. 23 (2021): 7960, https://doi.org/10.3390/s21237960.

[18] A. Afridi, S. Ullah, S. Khan, A. Ahmed, A. H. Khalil, and M. A. Tarar, "Design of Dual Band Wearable Antenna Using Metamaterials," *Journal of Microwave Power & Electromagnetic Energy* 47, no. 2 (2013): 126–137, https://doi.org/10.1080/08327823.2013.11689852.

[19] U. Ali, S. Ullah, J. Khan, et al., "Design and SAR Analysis of Wearable Antenna on Various Parts of Human Body, Using Conventional and Artificial Ground Planes," *Journal of Electrical Engineering and Technology* 12, no. 1 (2017): 317–328, https://doi.org/10.5370/JEET.2017.12.1.317.

[20] G. Tetik and E. Tetik, "Metamaterial Based Flexible Coplanar Antenna Design and Simulation for Human Body Applications," *Iğdır Üniversitesi Fen Bilimleri Enstitüsü Dergisi* 10, no. 4 (2020): 2541–2550, https://doi.org/10.21597/jist.689005.

[21] A. Y. I. Ashyap, Z. Zainal Abidin, S. H. Dahlan, H. A. Majid, and G. Saleh, "Metamaterial Inspired Fabric Antenna for Wearable Applications," *International Journal of RF and Microwave Computer-Aided Engineering* 29, no. 3 (March 2019): e21640, https://doi.org/10.1002/mmce.21640.

[22] A. Y. I. Ashyap, Z. Z. Abidin, S. H. Dahlan, and H. A. Majid, "Compact and Low-Profile Textile EBG-Based Antenna for Wearable Medical Appli Cations," *IEEE Antennas and Wireless Propagation Letters* 16 (2017): 2550–2553.

[23] B. Yin, J. Gu, X. Feng, B. Wang, Y. Yu, and W. Ruan, "A Low SAR Value Wearable Antenna for Wireless Body Area Network Based on AMC Structure," *Progress in Electromagnetics Research C* 95 (2019): 119–129, https://doi.org/10.2528/pierc19040103.

[24] G. S. Latha, G. S. N. Raju, and P. A. Sunny Dayal, "Design and Analysis Metamaterial Inspired Wearable Antenna for 2.45 GHz ISM Band," in *Proceedings 32nd International Conference on Microelectronics (ICM)* (December 2020), 1–4, https://doi.org/10.1109/icm50269.2020.9331772.

[25] P. Jha, A. Kumar, and A. De, "Two-Port Miniaturized Textile Antenna for 5G and WLAN Applications," *International Journal of Microwave and Wireless Technologies* 15, no. 8 (October 2023): 1443–1452, https://doi.org/10.1017/S175907872300020X.

[26] N. Sharma, P. Jha, M. Saxena, and D. Saxena, "DGS Based Eight-Port MIMO Antenna for 5G(N-79) and Sub-6 GHz Applications," in *2024 IEEE 11th Uttar Pradesh Section International Conference on Electrical, Electronics and Computer Engineering (UPCON)*, 1–4, https://doi.org/10.1109/UPCON62832.2024.10982784.

[27] A. Y. I. Ashyap, Z. Zainal Abidin, S. H. Dahlan, et al., "Compact and Low-Profile Textile EBG-Based Antenna for Wearable Medical Applications," *IEEE Antennas and Wireless Propagation Letters* 16 (2017): 2550–2553, https://doi.org/10.1109/lawp.2017.2732355.

[28] A. M. A. Waddah, N. R. Khairun, and M. S. Abdirahman, "Performance of Ultra-Wideband Wearable Antenna Under Severe Environmental Conditions and Specific Absorption Rate (SAR) Study at Near Distances," *ARPN Journal of Engineering and Applied Sciences* 10, no. 4 (2006).

[29] M. K. Khandelwal, B. K. Kanaujia, and S. Kumar, "Defected Ground Structure: Fundamentals, Analysis, and Applications in Modern Wireless Trends," *International Journal of Antennas and Propagation* 2017, no. 1 (2017): 1–22, https://doi.org/10.1155/2017/2018527.

[30] S. Das and D. Mitra, "A Compact Wideband Flexible Implantable Slot Antenna Design With Enhanced Gain," *IEEE Transactions on Antennas and Propagation* 66, no. 8 (August 2018): 4309–4314, https://doi.org/10.1109/tap.2018.2836463.

[31] S. Jam and H. Malekpoor, "Analysis on Wideband Patch Arrays Using Unequal Arms With Equivalent Circuit Model in X-Band," *IEEE Antennas and Wireless Propagation Letters* 15 (March 2016): 1861–1864, https://doi.org/10.1109/lawp.2016.2541179.

[32] Y. Lu, Y. Huang, H. T. Chattha, and P. Cao, "Reducing Ground-Plane Effects on UWB Monopole Antennas," *IEEE Antennas and Wireless Propagation Letters* 10 (February 2011): 147–150.

[33] "IEEE Standard for Safety Levels With Respect to Human Exposure to Radio Frequency Electromagnetic Fields, 3 kHz to 300 GHz" (1999).

[34] "IEEE Standard for Safety Levels With Respect to Human Exposure to Radio Frequency Electromagnetic Fields, 3 kHz to 300 GHz" (2005).

[35] R. E. Fields, "Evaluating Compliance With fcc Guidelines for Human Exposure to Radiofrequency Electromagnetic Fields," *Oet Bull* 65, no. 10 (1997): 1–57.

[36] E. T. E. Fields, "Guidelines for Limiting Human Exposure to Electromagnetic Fields up to 300 GHz" (2009).